Elastic scattering of electrons from dimethylsulfide and dimethylsulfoxide

K. C. Rao, K. G. Bhushan,* R. Mukund, S. C. Gadkari, and J. V. Yakhmi
Technical Physics and Prototype Engineering Division, Bhabha Atomic Research Center, Trombay, Mumbai 400 085, India
(Received 21 April 2009; revised manuscript received 5 May 2009; published 25 June 2009)

Differential cross sections for elastic scattering of electrons from dimethylsulfide and dimethylsulfoxide in the energy range from 30 to 500 eV are presented. The cross sections have been measured using a crossed-beam-type high-resolution electron spectrometer. The measured cross sections have been put on an absolute scale using the relative flow technique. The measured differential cross sections show an increase in the midangles at 30 and 50 eV for both the molecules that is characteristic of resonant enhanced *d*-wave scattering. Total and momentum-transfer cross sections were derived by integrating over all angles after extrapolating the data to forward and backward angles using a least-squares fitting procedure based on the Legendre polynomial expansion. Independent-atom-model-based theoretical calculations incorporating static, exchange, and polarization potentials are also reported and compared with the experimental cross sections. For energies lower than 100 eV, it is seen that the independent-atom-model calculations fail to predict the qualitative behavior of the differential cross sections correctly, while at energies greater than 100 eV it seems to describe the data adequately. The effect of polarization and enhancement of cross sections through *d*-wave scattering at low energies is also analyzed.

DOI: 10.1103/PhysRevA.79.062714 PACS number(s): 34.80.Bm, 34.10.+x

I. INTRODUCTION

Electron scattering by sulfur containing molecules is an interesting area of research for a multitude of reasons, the predominant being atmospheric and tropospheric chemistry. Several experimental and theoretical electron-scattering studies have been conducted on sulfur containing molecules in the recent past [1–4]. It has been observed that there is a similarity in the energy-dependent features of total-cross-section (TCS) curves for sulfur containing molecules where the sulfur atom is placed at the center of the molecule. The presence of sulfur, therefore, seems to strongly influence the overall qualitative behavior of the total and differential cross sections. Further, these studies also provide important differential and total cross-section data to test first-order theoretical models such as independent-atom-model (IAM)-based calculations [5].

Dimethylsulfide (DMS) is one of the principal volatile sulfur species found in sea water along with carbonyl sulfide and carbon disulfide [6]. DMS is generated as a result of biodegradation of organo-sulfur compounds in marine environments, through dimethyl-sulfoniopropionate (DMSP), a solute synthesized by phytoplankton for osmoregulation and cryoprotection [7]. Further, sulfur containing gases also affect the earth's radiative balance by direct scattering of solar radiation through the formation of sulfate aerosol particles [8]. Several studies have been conducted on DMS and its oxidation products in marine atmosphere and their distribution in surface waters [9,10]. Thompson *et al.* [11], Scott *et al.* [12], and more recently Limao-Vieira *et al.* [13] reported the vacuum-ultraviolet spectrum of DMS, while photoelectron spectra, photoionization spectra, electron momentum density distributions, transition polarizations, and fluorescence excitation have also been studied [14–19].

Dimethylsulfoxide is a highly polar water miscible solvent, commonly used in many pharmaceuticals due to its increased rate of absorption through organic tissues. It has been established from gas phase reactions that dimethylsulfoxide (DMSO) is produced by the oxidation of DMS with radicals such as OH and NO_3 among other products such as methanesulfonate and nonsea salt sulfates [20,21]. Sze *et al.* [22] studied the inner and valence shell excitation electronic spectra of DMSO using electron energy-loss spectroscopy and synchrotron-radiation-based x-ray photoabsorption techniques. Apart from photodissociation and energy distributions of fragmentation products that has been studied using vuv photons at different wavelengths [23,24], very little relevant literature exists for electron scattering from DMSO.

To our knowledge there have been no experimental or theoretical studies relating to electron scattering from DMS and DMSO. In this paper, we present the first measurements of absolute differential cross sections for the elastic scattering of electrons from DMS and DMSO using a high-resolution electron spectrometer. An IAM-based theoretical calculation using a two-potential coherent approach is also presented.

II. EXPERIMENT

A. Electron spectrometer

The electron spectrometer used in this experiment is of crossed-beam type and has been described in detail previ-

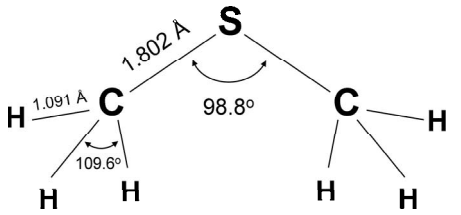

FIG. 1. Schematic structure of DMS molecule showing the bond lengths and bond angles [36] used in our IAM calculations.

*bhushan@barc.gov.in

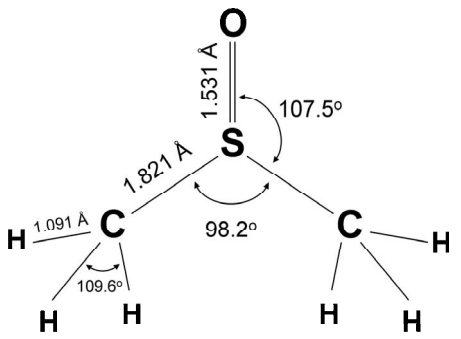

FIG. 2. Schematic structure of DMSO molecule showing the bond lengths and bond angles [37] used in our IAM calculations.

ously [3,25]; hence only a brief description is given here. Nearly monoenergetic electrons produced from an electron gun collide orthogonally with the target gas molecules introduced in the collision zone through a fine monochannel capillary tube. Elastically scattered electrons are energy analyzed with the help of two hemispherical energy analyzers that identically image the collision zone. The energy resolution of the analyzers is better than 0.2% of the incident-beam energy over the entire energy range of our present study. The scattering angle was calibrated by measuring the angular distribution for a well-known gas such as argon, at two different incident electron energies and matching the spectra with the known angular distributions. The same experiment was also used to calibrate the energy of the incident electron beam since the qualitative behavior of the angular distributions varies remarkably with the incident-beam energy. The energy analyzed electrons are detected by channeltron multipliers with nearly same efficiencies. The entire spectrometer is shielded by two layers of mu-metal sheet that reduces the ambient magnetic field to less than 5 milligauss and kept inside a vacuum chamber, pumped by a 500 l/s Turbomolecular pump giving a base pressure of about 2×10^{-8} mbar, which rises to about 5×10^{-7} mbar after introducing the target gas.

Angular distribution measurements are performed by rotating one energy analyzer over a given angular range, while the other is used as a monitor for the product of the number density of the target gas and the incident current. The measured parameters are related to the differential cross sections (DCS) as

$$\frac{d\sigma(E,\theta)}{d\Omega} = \frac{I_{sc}(E,\theta) - I_B(E,\theta)}{I_0 n_T l \Delta_\omega} \text{ cm}^2 \text{ sr}^{-1}, \quad (1)$$

where $I_{sc}(E,\theta)$ is the scattered electron current at a given energy and angle, $I_B(E,\theta)$ is the background electron counts at the same energy and angle, I_0 is the incident current, n_T is

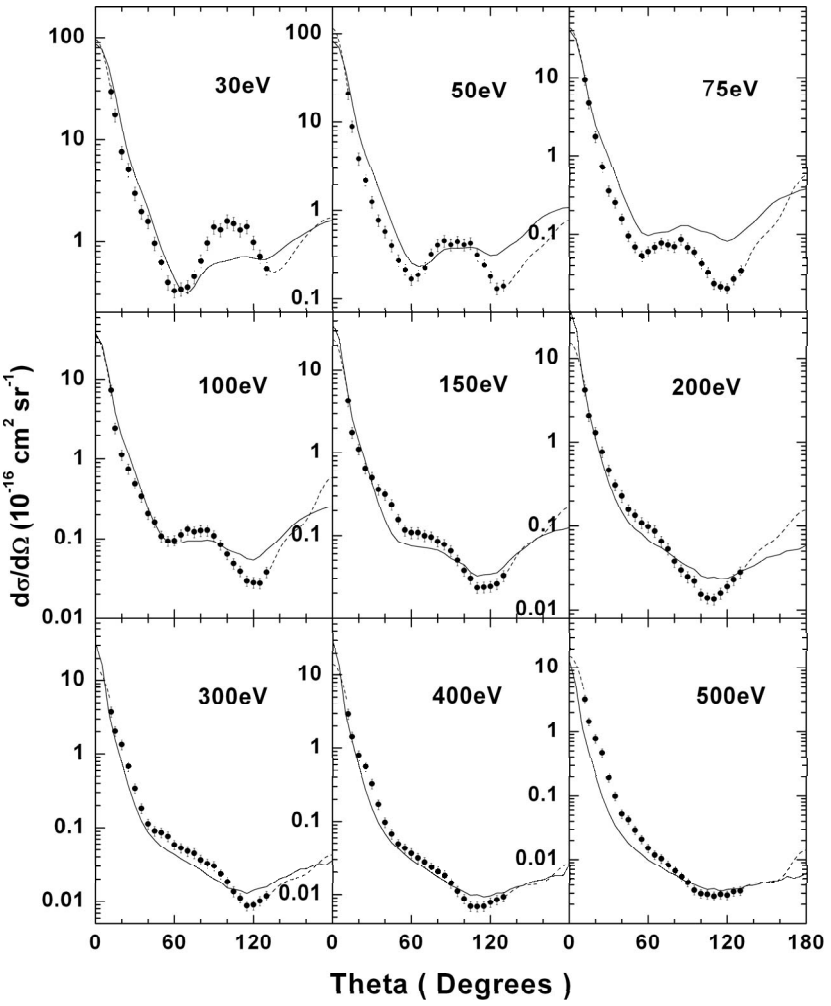

FIG. 3. Elastic differential cross sections for *e*-DMS scattering at different incident energies. The solid line is the theoretical calculation based on the IAM model and the dotted line on either side of the data points is the extrapolation based on Legendre polynomial fitting as given in the text.

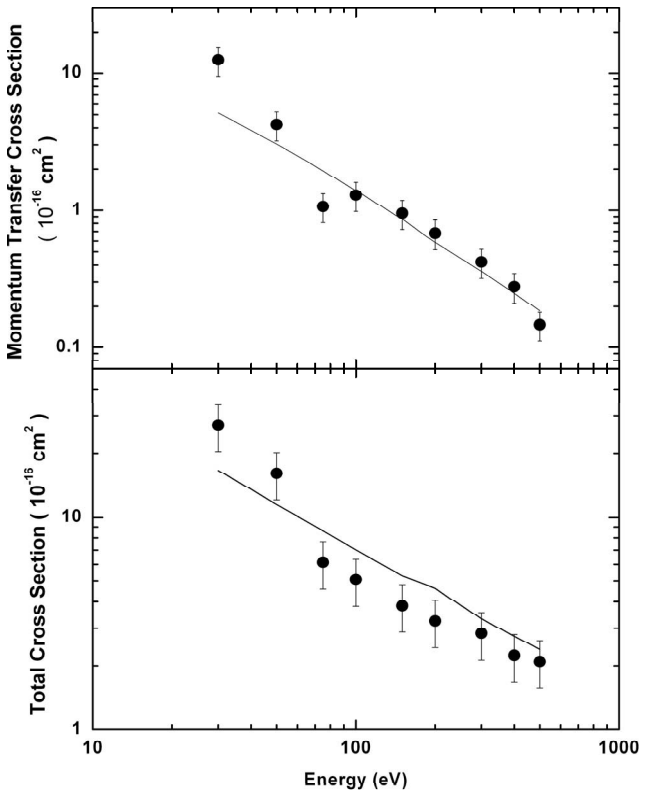

FIG. 4. Total-elastic and momentum-transfer cross sections for *e*-DMS scattering at different incident energies. The solid line is the theoretical calculation based on the IAM model.

the number density of the target gas, l is the path length, and Δ_ω is the solid angle subtended by the analyzers.

The measured relative DCS is put on an absolute scale using the relative flow technique [26] by using a standard calibration gas, argon in our case, whose cross sections have been measured accurately in the energy range of interest [27]. The absolute cross section for the gas under study is given by [28]

$$\left.\frac{d\sigma_g}{d\Omega}\right|_{(E,\theta)} = \frac{d\sigma_c(E,\theta)}{d\Omega}\left[\frac{N_c I_{oc}\sqrt{m_c}}{N_g I_{og}\sqrt{m_g}}\frac{I^s_{og}(E,\theta)}{I^s_{oc}(E,\theta)}\right] \text{ cm}^2 \text{ sr}^{-1}, \tag{2}$$

where N_c and N_g are the flow rates measured directly, I_{oc} and I_{og} are the incident electron currents during the respective measurements, I^s_{oc} and I^s_{og} are the scattered electron currents, m_c and m_g are the molecular masses, and σ_c and σ_g are the elastic cross sections of the calibration standard and the gas under study, respectively. A tenth-order Legendre-polynomial-based least-squares fit to the experimental data is utilized to extrapolate the data in the forward and backward angles. From this data, the total and momentum-transfer cross sections (MTCS) are calculated.

B. Experimental method

Pure DMS in liquid form at room temperature (vapor pressure at 25 °C is about 670 mbar [29]) was filled in a suitable metallic canister that could be cooled to liquid nitrogen temperatures. The canister was pumped continuously under frozen conditions to remove atmospheric gases and was allowed to reach room temperature naturally. Several such "freeze-pump-thaw" cycles were performed prior to letting the pure gas into the vacuum chamber. A residual gas analyzer was utilized to continuously monitor the partial pressure of the target gases in the vacuum chamber. A similar procedure was employed for DMSO also. However, since the vapor pressure of DMSO is much less than DMS (vapor pressure of DMSO at 25 °C is about 0.8 mbar [29]), the canister containing DMSO was heated to 50 °C and continuously pumped to increase the vapor pressure by nearly five times.

Measurement of absolute cross sections is a two-step process. In the first step, the relative DCS is measured accurately over the entire angular range. For this, all experiments were conducted in the preset normalized mode [3]. In this mode, any variation in the number density of the target gas molecules or the incident electron current is automatically corrected in the scattered electron count rates. Data were collected until the count statistics were better than 1%. In the second step, the relative cross sections were put on an absolute scale using the relative flow technique (mentioned in the previous section) by measuring absolute cross sections for argon (the calibration standard) at one particular angle by setting the flow rates for the target gas (DMS or DMSO in our case) and the calibration standard for identical Knudsen numbers.

C. Error analysis

The largest single source of error in these measurements is the calculation of the number density of the target gas, or in other words, the ratio of the flow rates for the gases under study. Since the flow control meter was not calibrated for all gases, calibration to the nearest available mass number was selected. In order to reduce this uncertainty, the absolute pressure at the reservoir was also measured simultaneously, from which the number density of the target gas could be independently estimated. The flow control meter and the absolute pressure measurement gauge are calibrated to better than 5% each. Thus from this data, it is estimated that the error in cross section due to the error in the measurement of flow rates to be less than 8%. Other errors arising due to counting statistics (1%), measurement of incident electron-beam current (<2%), gas pressure (<2%), and angular inaccuracy (<2%) are minimal. The error due to the possibility of other gases being present in the scattering zone is also negligible since a background subtraction was performed by letting the target gas from a side port in the vacuum chamber until the base pressure in the chamber reached the same pressure as when the target gas was flowing through the scattering center. This was further corroborated from the partial pressure data available through the residual gas analyzer measurements. Further, the spectrometer was also checked separately for multiple-scattering effects by measuring the angular distributions at two different pressures of the target and confirmed that there was no qualitative change in the

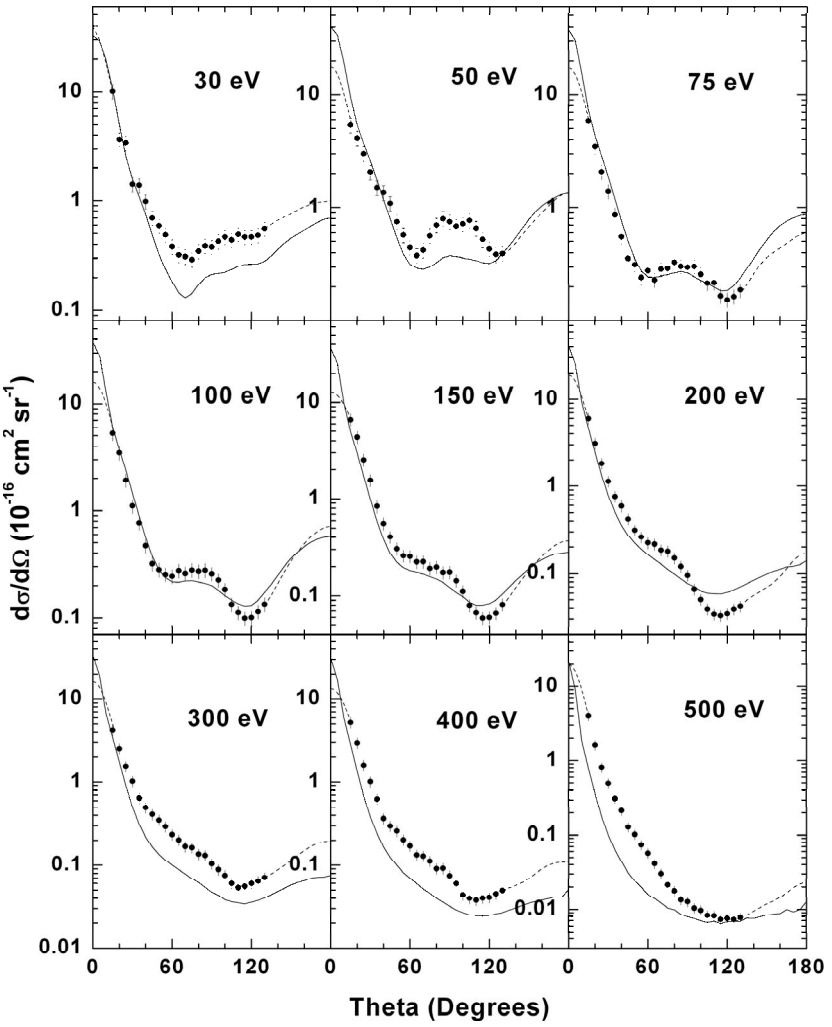

FIG. 5. Elastic differential cross sections for *e*-DMSO scattering at various incident energies. The solid line is the theoretical calculation based on the IAM model and the dotted line is the extrapolation from the Legendre polynomial fit to data.

angular distribution. Lastly, errors in the absolute cross sections of the calibration standard gas (in our case argon) also add to the overall error. Thus, it is estimated that the overall errors in the differential cross sections mentioned in this study for both DMS and DMSO are about 14%. The integral and momentum cross sections have slightly larger errors due to the extrapolation procedures employed to extract the DCS at 0° and 180°.

III. THEORY

Independent-atom-model-based calculations using the two-potential coherent approach of Hayashi and Kuchitsu [30] have been performed to generate DCS for *e*-DMS and *e*-DMSO scattering. The main aim of these calculations is to assist in explaining the qualitative behavior of the DCS in the intermediate energies (30–500 eV). The DCS averaged over all possible orientations of the molecular axis as predicted by the IAM is given by (excluding multiple-scattering terms) [31,32]

$$\frac{d\sigma}{d\Omega} = |f_{\mathrm{L}}|^2 + 2|f_{\mathrm{L}}|\sum_{i=1}^{N}|f_i|\cos(\eta_{\mathrm{L}} - \eta_i)\frac{\sin qR_i}{qR_i} + I_{\mathrm{S}} + I_{\mathrm{SS}}, \tag{3}$$

where f_i and f_{L} are the scattering amplitudes due to $V_i(r)$ (spherical short-range potential located at the i^{th} atom of the molecule) and due to $V_L(r)$ (long-range part of the interaction), q is the momentum transfer given by $q=2k\sin(\theta/2)$ with $k=\sqrt{2E}$ the wave number of incident electron of energy E and θ is the angle of scattering. R_i is the position vector of ith atom from the center of mass of the molecule, R_{ij} is the distance between ith and jth atom of the molecule, N is the total number of atoms present in the molecule,

$$I_{\mathrm{S}} = \sum_{i=1}^{N}|f_i|^2, \tag{4}$$

$$I_{\mathrm{SS}} = \sum_{i\neq j}^{N} f_i^* f_j \frac{\sin(qR_{ij})}{(qR_{ij})}, \tag{5}$$

and η in Eq. (3) is defined as $f=|f|e^{i\eta}$.

TABLE I. Measured differential cross sections for *e*-DMS elastic scattering. DCS's are in 10^{-16} cm^2 sr^{-1} units, while TCS's and MTCS's are in 10^{-16} cm^2 units derived after extrapolating the measured DCS's to 0° and 180°. See text for discussion.

	DCS (10^{-16} cm^2 sr^{-1})								
Angle	30 eV	50 eV	75 eV	100 eV	150 eV	200 eV	300 eV	400 eV	500 eV
15	1.74(1)[a]	8.91(0)	4.74(0)	2.46(0)	1.77(0)	2.06(0)	2.04(0)	1.43(0)	1.45(0)
20	7.52(0)	3.86(0)	1.77(0)	1.13(0)	1.10(0)	1.30(0)	1.33(0)	7.93(−1)	7.72(−1)
25	5.09(0)	2.23(0)	7.27(−1)	7.50(−1)	6.46(−1)	7.62(−1)	6.80(−1)	5.63(−1)	4.67(−1)
30	2.96(0)	1.25(0)	3.59(−1)	4.92(−1)	4.98(−1)	4.61(−1)	3.43(−1)	3.26(−1)	1.91(−1)
35	1.96(0)	7.76(−1)	2.53(−1)	3.40(−1)	3.60(−1)	3.07(−1)	1.84(−1)	1.71(−1)	9.89(−2)
40	1.57(0)	5.76(−1)	1.57(−1)	2.06(−1)	3.14(−1)	2.27(−1)	1.14(−1)	9.74(−2)	5.22(−2)
45	9.58(−1)	4.02(−1)	9.51(−2)	1.62(−1)	2.36(−1)	1.57(−1)	9.10(−2)	6.77(−2)	4.23(−2)
50	6.27(−1)	2.74(−1)	6.89(−2)	1.08(−1)	1.56(−1)	1.34(−1)	8.64(−2)	4.91(−2)	2.91(−2)
55	3.94(−1)	2.15(−1)	5.34(−2)	9.33(−2)	1.16(−1)	1.09(−1)	7.66(−2)	4.28(−2)	2.09(−2)
60	3.26(−1)	1.67(−1)	6.04(−2)	9.50(−2)	1.09(−1)	9.85(−2)	5.86(−2)	3.64(−2)	1.51(−2)
65	3.38(−1)	1.86(−1)	6.82(−2)	1.12(−1)	1.09(−1)	8.69(−2)	5.29(−2)	3.15(−2)	1.17(−2)
70	3.56(−1)	2.25(−1)	7.76(−2)	1.31(−1)	9.99(−2)	6.61(−2)	4.80(−2)	2.77(−2)	1.04(−2)
75	4.50(−1)	3.21(−1)	7.35(−2)	1.22(−1)	9.61(−2)	5.32(−2)	4.48(−2)	2.34(−2)	8.20(−3)
80	6.44(−1)	4.06(−1)	6.95(−2)	1.26(−1)	8.52(−2)	3.77(−2)	3.65(−2)	2.04(−2)	6.70(−3)
85	9.64(−1)	4.55(−1)	8.61(−2)	1.27(−1)	7.81(−2)	2.97(−2)	3.25(−2)	1.81(−2)	5.40(−3)
90	1.39(0)	4.11(−1)	6.78(−2)	1.09(−1)	6.50(−2)	2.47(−2)	3.02(−2)	1.42(−2)	4.40(−3)
95	1.30(0)	4.45(−1)	5.90(−2)	8.40(−2)	5.00(−2)	2.21(−2)	2.36(−2)	1.11(−2)	3.30(−3)
100	1.59(0)	4.11(−1)	4.27(−2)	6.37(−2)	3.76(−2)	1.54(−2)	1.84(−2)	8.80(−3)	3.00(−3)
105	1.50(0)	4.28(−1)	3.25(−2)	4.83(−2)	3.01(−2)	1.39(−2)	1.36(−2)	6.90(−3)	2.90(−3)
110	1.30(0)	3.15(−1)	2.33(−2)	3.87(−2)	2.34(−2)	1.35(−2)	1.11(−2)	6.80(−3)	2.70(−3)
115	1.40(0)	2.42(−1)	2.13(−2)	2.94(−2)	2.37(−2)	1.58(−2)	8.70(−3)	6.90(−3)	2.90(−3)
120	9.81(−1)	1.78(−1)	2.03(−2)	2.79(−2)	2.41(−2)	1.90(−2)	9.00(−3)	7.90(−3)	2.80(−3)
125	6.30(−1)	1.30(−1)	2.65(−2)	2.75(−2)	2.61(−2)	2.30(−2)	1.02(−2)	8.50(−3)	3.20(−3)
130	4.64(−1)	1.39(−1)	3.45(−2)	3.78(−2)	3.25(−2)	2.80(−2)	1.19(−2)	9.40(−3)	3.30(−3)
Error	16%	16%	14%	13%	14%	14%	14%	14%	14%
TCS	27.12	16.1	6.12	5.08	3.83	3.24	2.83	2.23	2.09
Error	24%	24%	25%	24%	24%	22%	22%	22%	22%
MTCS	12.49	4.22	1.07	1.29	0.95	0.68	0.42	0.28	0.15
Error	28%	28%	26%	26%	24%	24%	24%	24%	24%

[a]1.74(1) means 1.74×10^{1}.

The electron-molecule interaction potential used in our present calculations is of the form

$$V(r) = V_i(r) + V_L(r), \tag{6}$$

where $V_i(r)=V_{\mathrm{Stat}}(r)+V_{\mathrm{Exch}}(r)$, $V_L(r)=V_{\mathrm{Polz}}(r)\cdot V_{\mathrm{Stat}}(r)$ is the static interaction potential, $V_{\mathrm{Exch}}(r)$ is the exchange potential similar to Hara's "free electron gas exchange model" [33] which is an energy-dependent potential, and $V_{\mathrm{Polz}}(r)$ is the polarization potential as given by Zhang *et al.* [34]. The charge densities $\rho(r)$ required to evaluate the potentials of constituent atoms have been derived from the Hartree-Fock wave functions of Bunge and Barrientos [35]. Phase shifts were generated separately for the short-range part $V_i(r)$ and the long part $V_L(r)$ and were used in Eq. (3) accordingly to calculate the atomic scattering amplitudes and hence the differential cross sections. The values for the bond length and the bond angles for DMS and DMSO used in our present IAM calculations are shown schematically in Figs. 1 and 2 [36,37].

IV. RESULTS AND DISCUSSION

A. Differential cross sections for DMS

Figure 3 shows the measured absolute DCS for DMS in the energy range 30–500 eV. DCS computed from independent-atom-model-based theoretical calculations are also shown for comparison. Legendre polynomial extrapolations to the data are also shown in the figure. The measured

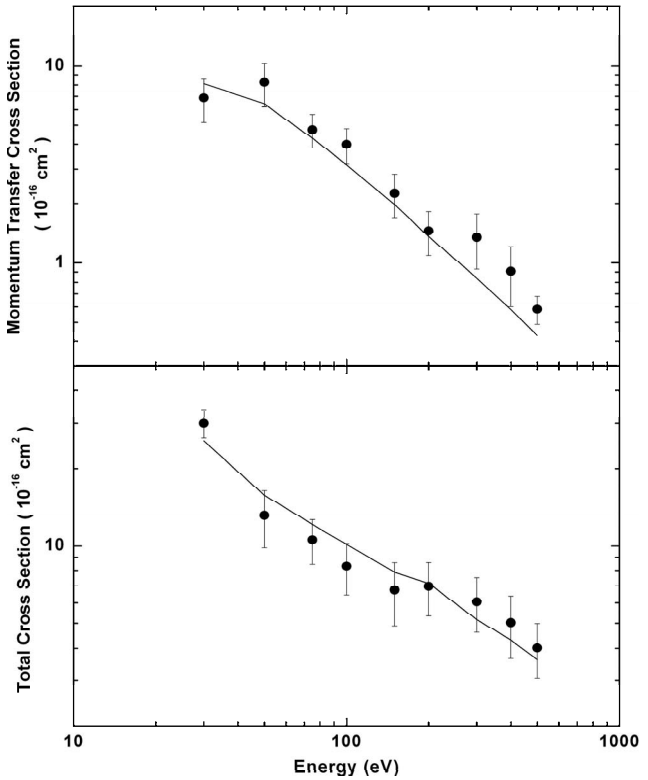

FIG. 6. Total elastic and Momentum transfer cross sections for *e*-DMSO scattering at different incident energies. The solid line is the theoretical calculation based on the IAM model.

DCS values are also given in Table I. An increase in cross section is observed at energies 30 and 50 eV in the angular range 30 to 90°. Experimental artifacts such as multiple-scattering effects have been ruled out by repeating the experiment at different target number densities and different incident electron currents. The resolution of the present experimental setup is high enough to distinguish between ground state and the first dipole allowed electronic excitation, $1\ ^1B_1 \leftarrow X\ ^1A_1$, which is estimated to be 5.58 eV [38]. However, the resolution is insufficient to reject vibrational and rotational excitations. The measured cross sections, therefore, could include a small percentage of ro-vibrational excitations. DMS is a bent molecule where in the sulfur atom is shielded by the methyl radicals, and since hydrogen is a weak scatterer, for practical purposes, DMS can be considered as a tri-atomic molecule of the form C-S-C. Comparisons with other sulfur containing tri-atomic molecules such as OCS or CS_2 indicate no increase in the cross section as observed for DMS at these energies and angles partly because these are linear molecules unlike DMS.

The possibility of a resonant enhanced d-wave scattering cannot be ruled out. Low energy σ^* shape resonances observed in DMS [39] have been attributed primarily to the formation of $(CH_3)_2S^-$ anion. At higher energies, the nature of electron-DMS interaction as predicted by the shape of the potential has a notable 3*d* character and hence a *d*-wave enhancement will increase the cross section values through the midangles as observed in our present experiment for energies 30 and 50 eV. However, at present, there are no theoretical calculations available incorporating enhancements of *d*-wave character through a shape resonance in order to verify this phenomenon.

Figure 4 shows the experimental TCS and MTCS at various incident energies obtained by extrapolating the cross sections to 0° and 180° and integrating over all angles. At 30 and 50 eV, the cross sections predicted by the IAM theory are lower by nearly a factor of 1.5 than the experimental cross sections. For energies greater than 75 eV the IAM calculations overestimate the experimental TCS, while the experimental MTCS agree reasonably well. The higher error bars (22%) in the TCS and (24%) MTCS are mainly due to the extrapolation of the experimental data to 0° and 180°. It can be seen that for incident energies above 100 eV, the experimental data agrees with IAM calculations quite satisfactorily. For energies below 100 eV, the experimental cross sections differ quite strongly with the IAM calculations. The present calculations incorporating static, exchange, and polarization potential fails to predict the features observed in the DCS data at low energies. The role of polarization can be seen clearly in the experimental data where the cross sections predicted by the IAM theory overestimate at low energies and underestimate at higher energies. An energy-dependent polarization function as suggested by Garcia and Blanco [40], of the form $\sigma_p=(xZ+y\alpha)E^{-\delta}$, where x and y are free parameters, Z is the number of target electrons, α is the molecular polarizability, E is the energy of the incident electron (in keV), and $\delta<1$, could be incorporated in the theoretical calculations to better understand this effect.

B. Differential cross sections for DMSO

Figure 5 shows the measured absolute DCS for DMSO in the energy range 30–500 eV. DCS computed from independent-atom-model-based theoretical calculations are also shown for comparison. Table II gives the measured DCS values for DMSO. Unlike DMS, an increase in DCS is observed only in 50 eV, whereas at 30 eV even though the experimental cross sections are much higher than the theoretical cross sections, the qualitative behavior nearly follows the theoretical cross sections. DMSO is a highly polar molecule (dipole moment of 3.96 D [41]), in many ways similar to a water molecule. Comparison of DCS of DMSO with the recently published data on DCS of H_2O by Khakoo *et al.* [42] at low energies (30 and 50 eV) shows a different qualitative behavior for DMSO. At 50 eV, the observed DCS exhibits a strong *d*-wave character possibly due to a broad shape resonance similar to DMS that is not predicted by our IAM calculations. The qualitative behavior of the cross section although seems to be strongly influenced by the sulfur atom, the highly polar nature of the molecule enhances dipole scattering at 30 eV unlike DMS. At 50 eV, polarizability plays a lesser part and hence there is a *d*-wave enhancement to the cross section through the midangles. Theoretical calculations incorporating an energy-dependent polarization potential and enhancements of *d*-wave character will help in further understanding the nature of *e*-DMSO reaction at these energies.

A clear minimum is seen in the DCS for energies 100, 150, and 200 eV which is again not predicted by the IAM

TABLE II. Measured differential cross sections for *e*-DMSO elastic scattering. DCS's are in 10^{-16} cm^2 sr^{-1} units, while TCS's and MTCS's are in 10^{-16} cm^2 units derived after extrapolating the measured DCS's to 0° and 180°. See text for discussion.

	DCS (10^{-16} cm^2 sr^{-1})								
Angle	30 eV	50 eV	75 eV	100 eV	150 eV	200 eV	300 eV	400 eV	500 eV
15	1.01(1)[a]	5.41(0)	5.86(0)	5.28(0)	6.60(0)	5.99(0)	4.21(0)	5.22(0)	4.02(0)
20	3.65(0)	4.12(0)	3.46(0)	3.47(0)	4.35(0)	3.10(0)	2.52(0)	2.94(0)	1.62(0)
25	3.40(0)	3.01(0)	2.08(0)	1.92(0)	2.53(0)	1.82(0)	1.54(0)	1.58(0)	8.09(−1)
30	1.42(0)	2.07(0)	1.39(0)	1.10(0)	1.56(0)	1.13(0)	1.02(0)	1.01(0)	4.94(−1)
35	1.39(0)	1.50(0)	8.63(−1)	7.73(−1)	8.38(−1)	7.59(−1)	6.45(−1)	6.26(−1)	3.11(−1)
40	9.85(−1)	1.36(0)	5.50(−1)	4.68(−1)	5.60(−1)	5.91(−1)	4.96(−1)	3.66(−1)	2.14(−1)
45	6.94(−1)	1.09(0)	3.56(−1)	3.18(−1)	4.04(−1)	4.23(−1)	4.12(−1)	2.97(−1)	1.29(−1)
50	5.90(−1)	7.49(−1)	3.13(−1)	2.80(−1)	3.05(−1)	3.14(−1)	3.51(−1)	2.58(−1)	1.02(−1)
55	4.87(−1)	5.71(−1)	2.41(−1)	2.54(−1)	2.58(−1)	2.60(−1)	2.93(−1)	2.03(−1)	7.39(−2)
60	3.80(−1)	4.43(−1)	2.77(−1)	2.45(−1)	2.54(−1)	2.22(−1)	2.34(−1)	1.71(−1)	5.70(−2)
65	3.20(−1)	3.78(−1)	2.30(−1)	2.75(−1)	2.23(−1)	2.15(−1)	2.02(−1)	1.33(−1)	4.12(−2)
70	3.09(−1)	4.21(−1)	2.85(−1)	2.59(−1)	2.24(−1)	1.84(−1)	1.68(−1)	1.29(−1)	3.04(−2)
75	2.90(−1)	5.62(−1)	2.91(−1)	2.78(−1)	1.92(−1)	1.78(−1)	1.63(−1)	1.12(−1)	2.14(−2)
80	3.45(−1)	7.00(−1)	3.29(−1)	2.72(−1)	1.98(−1)	1.49(−1)	1.36(−1)	9.10(−2)	1.78(−2)
85	3.86(−1)	7.96(−1)	3.03(−1)	2.77(−1)	1.74(−1)	1.19(−1)	1.31(−1)	9.16(−2)	1.34(−2)
90	3.77(−1)	7.50(−1)	2.97(−1)	2.57(−1)	1.76(−1)	9.52(−2)	1.04(−1)	7.47(−2)	1.26(−2)
95	4.24(−1)	6.82(−1)	3.03(−1)	2.25(−1)	1.43(−1)	6.62(−2)	8.85(−2)	5.99(−2)	1.04(−2)
100	4.64(−1)	7.15(−1)	2.58(−1)	1.84(−1)	1.11(−1)	5.03(−2)	7.54(−2)	4.38(−2)	9.71(−3)
105	4.37(−1)	7.69(−1)	2.15(−1)	1.33(−1)	7.97(−2)	3.90(−2)	6.01(−2)	3.99(−2)	8.29(−3)
110	4.92(−1)	6.53(−1)	2.17(−1)	1.12(−1)	6.71(−2)	3.41(−2)	5.37(−2)	3.79(−2)	8.20(−3)
115	4.64(−1)	5.22(−1)	1.66(−1)	9.90(−2)	5.89(−2)	3.28(−2)	5.56(−2)	4.02(−2)	7.26(−3)
120	4.65(−1)	4.31(−1)	1.53(−1)	1.00(−1)	5.99(−2)	3.46(−2)	6.01(−2)	4.09(−2)	7.49(−3)
125	4.81(−1)	3.85(−1)	1.63(−1)	1.14(−1)	6.63(−2)	3.90(−2)	6.42(−2)	4.51(−2)	7.26(−3)
130	5.55(−1)	3.92(−1)	1.88(−1)	1.34(−1)	8.13(−2)	4.21(−2)	7.08(−2)	4.95(−2)	7.74(−3)
Error	18%	16%	14%	14%	14%	14%	14%	14%	14%
TCS	30.05	13.11	10.56	8.33	6.74	6.97	6.07	5.02	4.02
Error	18%	18%	16%	15%	16%	16%	16%	16%	16%
MTCS	6.87	8.26	4.74	3.99	2.26	1.46	1.35	0.91	0.58
Error	18%	18%	16%	15%	16%	16%	16%	16%	16%

[a]1.01(1) means 1.01×10^1.

calculations. It can be seen that the experimental data for 75 and 100 eV show satisfactory qualitative agreement with IAM calculations, while at all other higher energies the IAM calculations with polarization potential underestimate the experimental DCS. This is understandable since the polarization potential used in the IAM calculations is not energy dependent and purely depends on the molecular polarizability and hence its effect is to reduce the overall cross section.

Figure 6 shows the experimental TCS and MTCS for electron-DMSO scattering at various incident energies. In general, better agreement with the IAM calculations is found for TCS and MTCS as compared to DMS cross sections. The errors in the TCS and MTCS are 22% and 24% respectively, largely due to the extrapolation of DCS data in the forward and backward angles. The TCS data shows a shift at 200 eV above which the IAM model underestimates the experimental cross sections. Thus, it can be seen that while dipole scattering dominates in the forward angles at low energies, the intermediate and backward angle scattering is largely attributed to the size of the molecule.

V. CONCLUSION

Experimental differential cross sections for elastic scattering of electrons from DMS and DMSO have been reported, measured using a high-resolution crossed-beam-type electron spectrometer. Total and momentum-transfer cross sections calculated by extrapolating the angle-limited DCS data are also reported. An IAM-based theoretical calculation employing static, exchange, and polarization potentials has been

presented as a guide to understanding the qualitative behavior of the measured DCS. A large increase in cross section is noticed at low energies and at intermediate angles for the both the molecules, which is characteristic of *d*-wave scattering through the decay of shape resonance. At low energies, the qualitative behavior of the IAM-based theoretical DCS deviate considerably from the measured DCS. It is suggested that theoretical calculations incorporating *d*-wave enhancements to the scattering amplitude, valence-bond distortion, and energy-dependent polarization functions can help understand the nature of electron-molecule interaction better, while at higher energies the IAM calculations with static, exchange, and polarization potentials seem to describe the cross-section behavior adequately.

ACKNOWLEDGMENTS

This work was supported by Dept. of Atomic Energy, Govt. of India, through project grant "Programme on Advanced Analytical and Other Instruments." The authors would like to thank Professor Minaxi Vinodkumar and K. Korot, Department of Physics, V.P.&R.P.T.P. Science College, Vallabh Vidyanagar, Gujarat, India, for providing the atomic phase shifts used in our IAM calculations. Technical help of S. M. Rodrigues for the assembly and alignment of the electron spectrometer is gratefully acknowledged.

[1] C. Szmytkowski, P. Mozejko, S. Kwitnewski, E. Ptasinska-Denga, and A. Domaracka, J. Phys. B **38**, 2945 (2005).
[2] S. E. Michelin, T. Kroin, I. Iga, M. G. P. Homem, H. S. Miglio, and M. T. Lee, J. Phys. B **33**, 3293 (2000).
[3] K. G. Bhushan, K. C. Rao, S. C. Gadkari, J. V. Yakhmi, and S. K. Gupta, Phys. Rev. A **79**, 012702 (2009).
[4] Deo Raj and S. Tomar, J. Phys. B **30**, 1989 (1997).
[5] M. J. Brunger and S. J. Buckman, Phys. Rep. **357**, 215 (2002).
[6] P. S. Liss, A. D. Hatton, G. Malin, P. D. Nightingale, and S. M. Turner, Philos. Trans. R. Soc. London, Ser. B **352**, 159 (1997).
[7] R. Simo, A. D. Hatton, G. Malin, and P. S. Liss, Mar. Ecol.: Prog. Ser. **167**, 291 (1998).
[8] R. J. Charlson *et al.*, Science **225**, 423 (1992).
[9] G. P. Ayers *et al.*, Netherlands J. Sea Res. **43**, 275 (2000).
[10] M. A. Cerqueira and C. A. Pio, Atmos. Environ. **33**, 3355 (1999).
[11] S. D. Thompson, D. G. Carroll, F. Watson, M. O'Donnell, and S. P. McGlynn, J. Chem. Phys. **45**, 1367 (1966).
[12] J. D. Scott, G. C. Causley, and B. R. Russell, J. Chem. Phys. **59**, 6577 (1973).
[13] P. Limao-Vieira, S. Eden, P. A. Kendall, N. J. Mason, and S. V. Hoffmann, Chem. Phys. Lett. **366**, 343 (2002).
[14] D. C. Frost, F. G. Herring, A. Katrib, C. A. McDowell, and R. A. N. McLean, J. Phys. Chem. **76**, 1030 (1972).
[15] A. Schweig and W. Thiel, Mol. Phys. **265**, 265 (1974).
[16] F. C. Chang, V. Y. Young, J. W. Prather, and K. L. Cheng, J. Electron Spectrosc. Relat. Phenom. **40**, 363 (1986).
[17] P. Quintana, R. F. Delmdahl, D. H. Parker, B. Martınez-Haya, F. J. Aoiz, L. Banares, and E. Verdasco, Chem. Phys. Lett. **325**, 146 (2000).
[18] B. Martınez-Haya, P. Quintana, L. Banares, P. Samartiz, D. J. Smith, and T. N. Kitsopoulos, J. Chem. Phys. **114**, 4450 (2001).
[19] Y. Zheng, J. Rolke, G. Cooper, and C. E. Brion, J. Electron Spectrosc. Relat. Phenom. **123**, 377 (2002).
[20] G. S. Tyndall and A. R. Ravishankara, Int. J. Chem. Kinet. **23**, 483 (1991).
[21] H. Falbe-Hansen, S. Sorensen, N. R. Jensen, T. Pedersen, and J. Hjorth, Atmos. Environ. **34**, 1543 (2000).
[22] K. H. Sze, C. E. Brion, M. Tronc, S. Bodeur, and A. P. Hitchcock, Chem. Phys. **121**, 279 (1988).
[23] D. A. Blank, S. W. North, D. Stranges, A. G. Suits, and Y. T. Lee, J. Chem. Phys. **106**, 539 (1997).
[24] Gail M. Thorson, Christopher M. Cheatum, Martin J. Coffey, and F. Fleming Crim, J. Chem. Phys. **110**, 10843 (1999).
[25] K. C. Rao, K. G. Bhushan, S. C. Gadkari, and J. V. Yakhmi, Asian J. Phys. **16**, 353 (2007).
[26] S. K. Srivastava, S. Trajmar, A. Chutjian, and W. Williams, J. Chem. Phys. **63**, 2659 (1975).
[27] R. H. J. Jansen, F. J. de Heer, H. J. Luyken, B. van Wingerden, and H. J. Blaauw, J. Phys. B **9**, 185 (1976).
[28] J. C. Nickel, C. Mott, I. Kanik, and D. C. McCollum, J. Phys. B **21**, 1867 (1988).
[29] T. E. Daubert and R. P. Danner, *Physical and Thermodynamic Properties of Pure Chemicals Data Compilation* (Taylor and Francis, Washington, DC, 1989).
[30] S. Hayashi and K. Kuchitsu, J. Phys. Soc. Jpn. **41**, 1724 (1976).
[31] S. P. Khare, D. Raj, and Piyush Sinha, J. Phys. B **27**, 2569 (1994).
[32] A. Jain and S. S. Tayal, J. Phys. B **15**, L867 (1982).
[33] S. Hara, J. Phys. Soc. Jpn. **22**, 710 (1967).
[34] X. Zhang, J. Sun, and Y. Liu, J. Phys. B **25**, 1893 (1992).
[35] C. F. Bunge and J. A. Barrientos, At. Data Nucl. Data Tables **53**, 113 (1993).
[36] Louis Pierce and Michiro Hayashi, J. Chem. Phys. **35**, 479 (1961).
[37] R. Thomas, Clara Brink Shoemaker, and Klaas Eriks, Acta Crystallogr. **21**, 12 (1966).
[38] V. Pérez Mondéjar, M. J. Yusá, I. García Cuesta, A. M. J. Sanchez de Merás, and J. Sánchez-Marín, Theor. Chem. Acc. **118**, 527 (2007).
[39] C. Dezarnaud-Dandine, F. Bournel, M. Tronc, D. Jones, and A. Modelli, J. Phys. B **31**, L497 (1998).
[40] G. García and F. Blanco, Phys. Lett. A **279**, 61 (2001).
[41] A. L. McClellan, *Tables of Experimental Dipole Moments* (Rahara Enterprises, California, 1974), Vol. 2.
[42] M. A. Khakoo, H. Silva, J. Muse, M. C. A. Lopes, C. Winstead, and V. McKoy, Phys. Rev. A **78**, 052710 (2008).